Supporting Information

High-Temperature Flexible Supercapacitor Based on Pseudocapacitive Behavior of FeOOH in Ionic Liquid Electrolyte

Baoshou Shen,[a,b] Ruisheng Guo,[a] Junwei Lang,[a] Li Liu,[a,b] Lingyang Liu[a] and Xingbin Yan*[a]

[a] Laboratory of Clean Energy Chemistry and Materials, State Key Laboratory of Solid Lubrication, Lanzhou Institute of Chemical Physics, Chinese of Academy of Sciences, Lanzhou, 730000, P.R. China

[b] University of Chinese Academy of Sciences, Beijing, 100039, P.R. China.

* Corresponding author. Tel.: +86-931-4968055; fax: +86-931-4968055. E-mail address: xbyan@licp.cas.cn

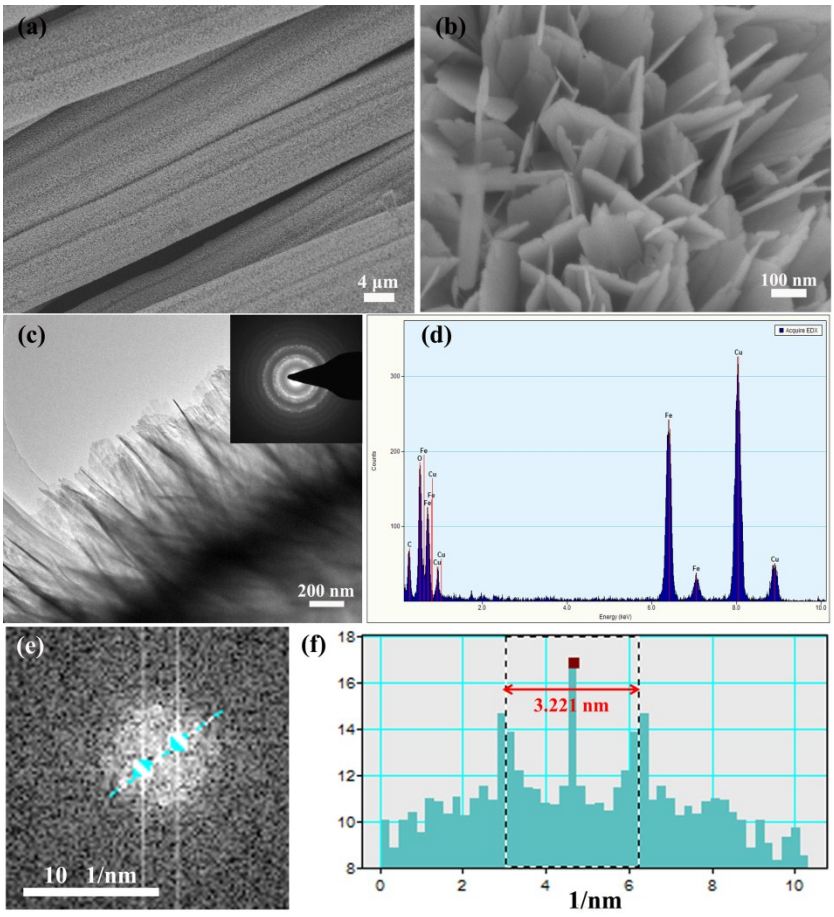

Figure S1. (a and b) SEM images of the FeOOH NSs/CC electrode with low and high magnifications. (c) TEM image of FeOOH NSs. Inset is the corresponding SAED pattern. (d) EDX spectrum of FeOOH NSs. And the C element and Cu element originated from carbon coated copper mesh. (e and f) the Fast Fourier Transforms (FFT) patterns of Figure 1 (c) (inset image) and corresponding line profiles from marked areas of a lattice-resolved high-resolution TEM image.

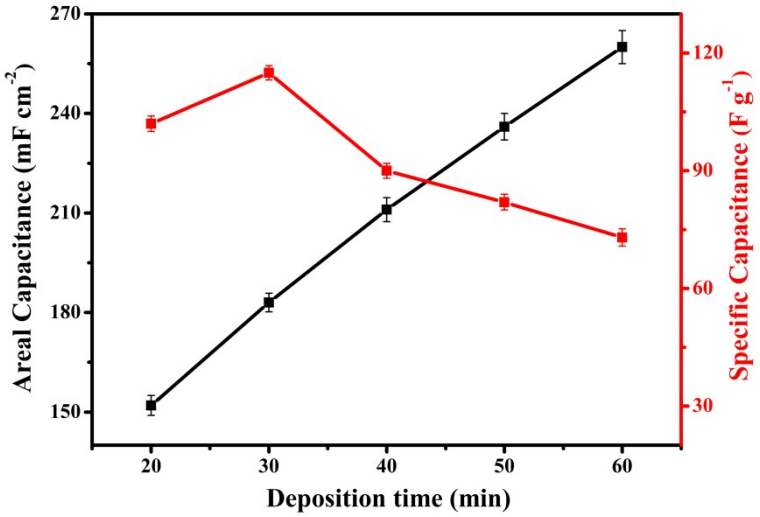

Figure S2. Gravimetric capacitance and areal capacitance of FeOOH NSs/CC electrode as a function of deposition time.

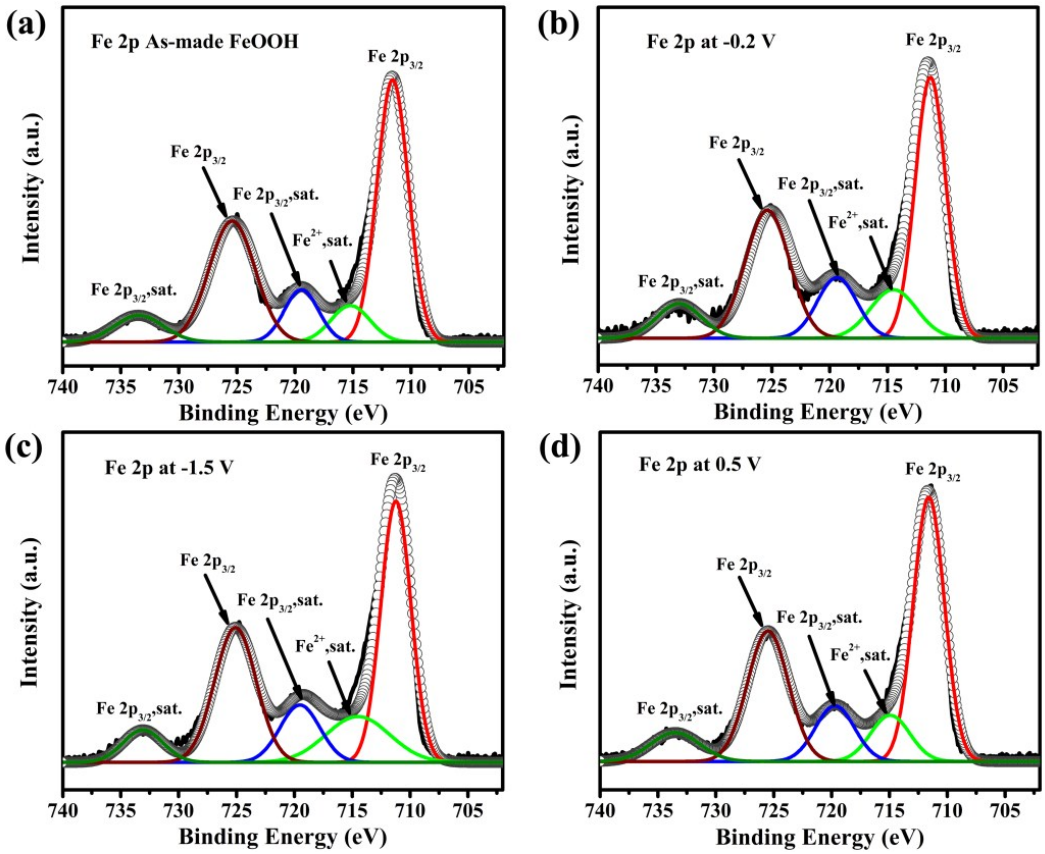

Figure S3. Well-fitted XPS Fe 2p spectra of the FeOOH electrode in EMIM-NTF_2 IL with respect to applied potentials from −1.5 to 0.5 V (black solid lines are experimental data, the dark gray hollow lines are fitted results).

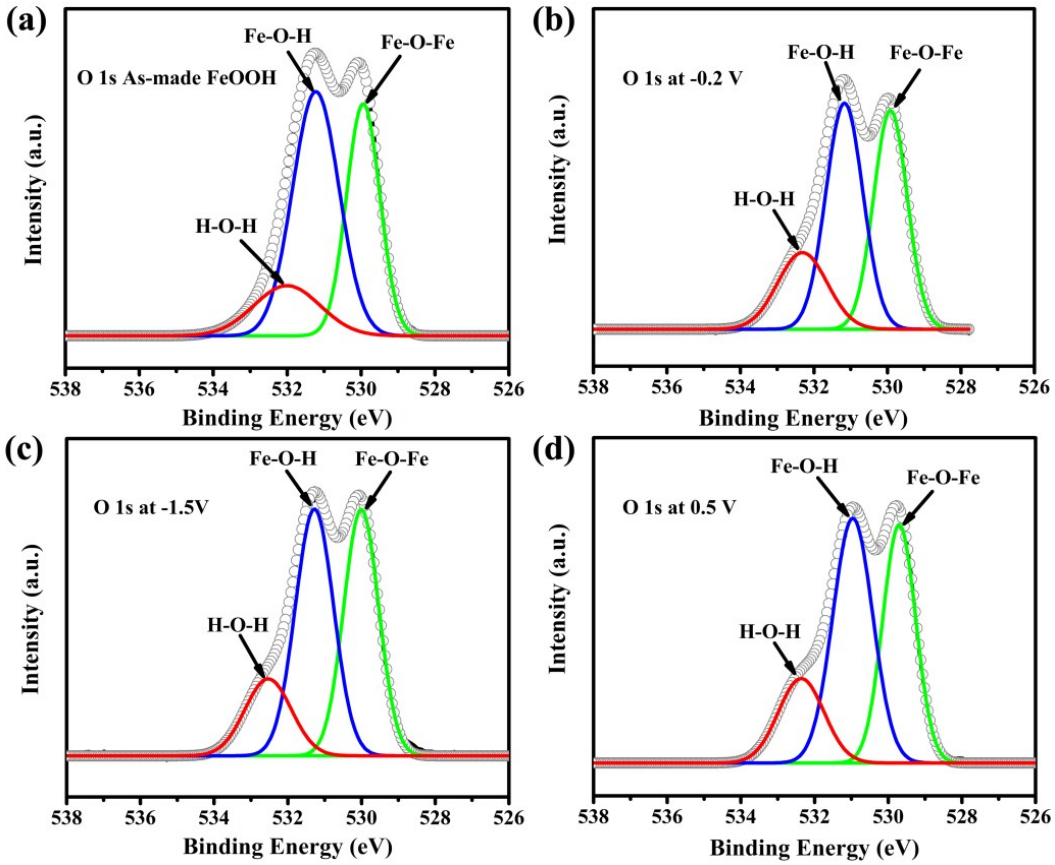

Figure S4. Well-fitted XPS O 1s spectra of the FeOOH electrode in EMIMNTF$_2$ electrolyte with respect to applied potentials from −1.5 to 0.5 V (black solid lines are experimental data, the dark gray hollow lines are fitted results).

Table S1. Peak position and atom contents of Fe^{2+},sat (light-gray region in table) based on deconvoluted XPS Fe 2p spectra (Figure S3) and peak positions and atom contents based on deconvoluted XPS O 1s spectra (Figure S4) of the FeOOH electrode during dischage and charge process.

	Peak position (±0.2 eV)	**As-made FeOOH (atm%)**	**Dischage at -1.5 V (atm%)**	**Charge at 0.5 V (atm%)**
Fe^{2+},sat	715.1	6.4	14.5	9.3
Fe-O-Fe	529.9	35.6	40.8	37.3
Fe-OH	531.2	50.1	42.5	46.2
H-OH	532.2	12.3	16.7	15.5

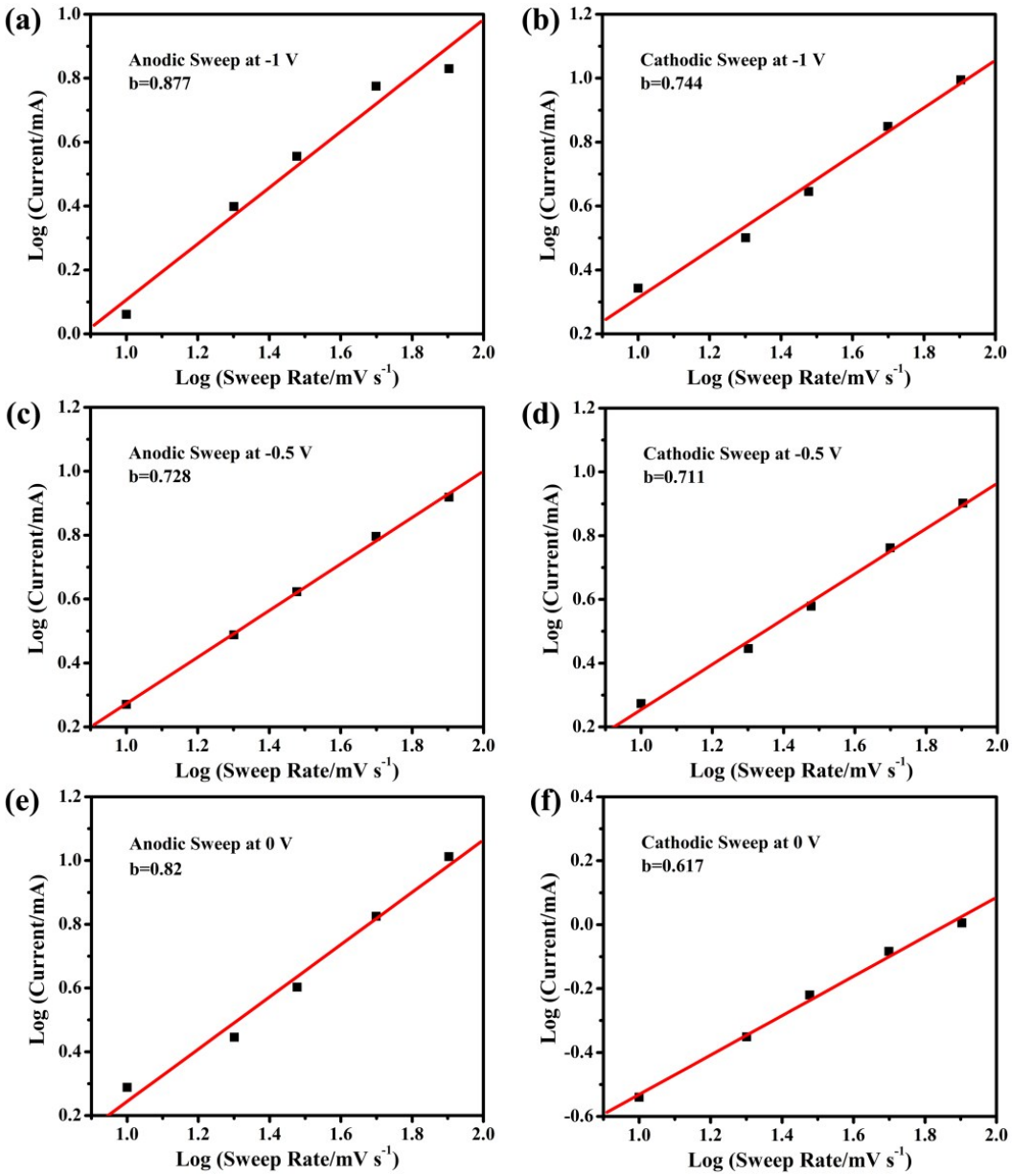

Figure S5. Calculated *b*-values for the FeOOH NSs/CC electrode corresponding to the cathodic ($[EMIM]^+$ insertion) and anodic sweep ($[EMIM]^+$ extraction) at the potentials of -1V, -0.5 V and 0 V with different sweep rates.

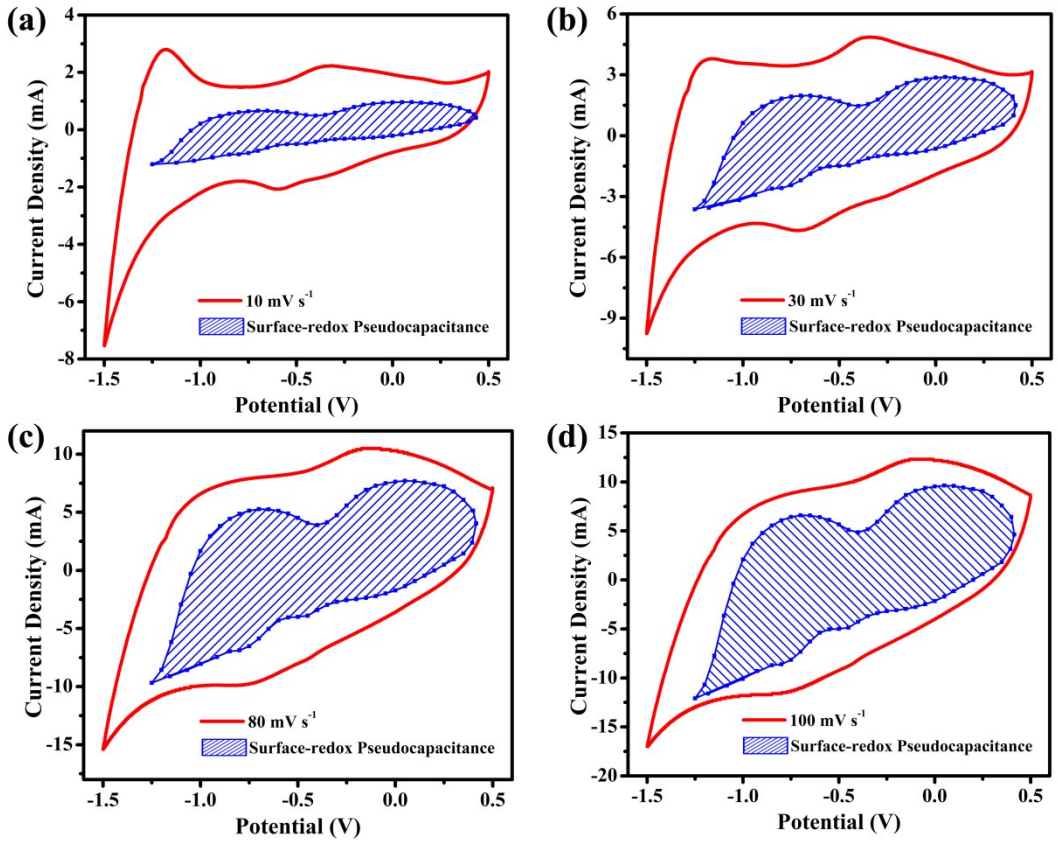

Figure S6. Voltammetric response for the FeOOH NSs/CC electrode at different sweep rates with shaded region representing surface-redox pseudocapacitance.

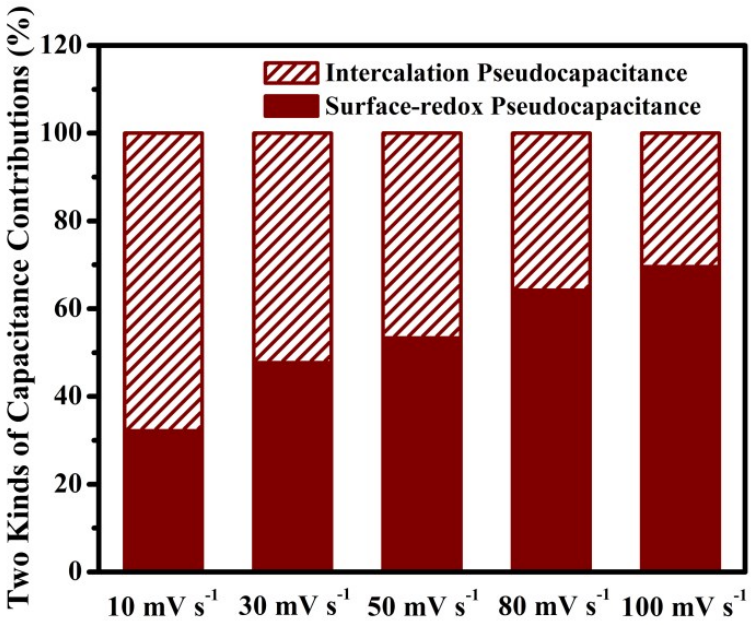

Figure S7. Two kinds of pseudocapacitance contributions at different sweep rates in EMIM-NTF_2 IL.

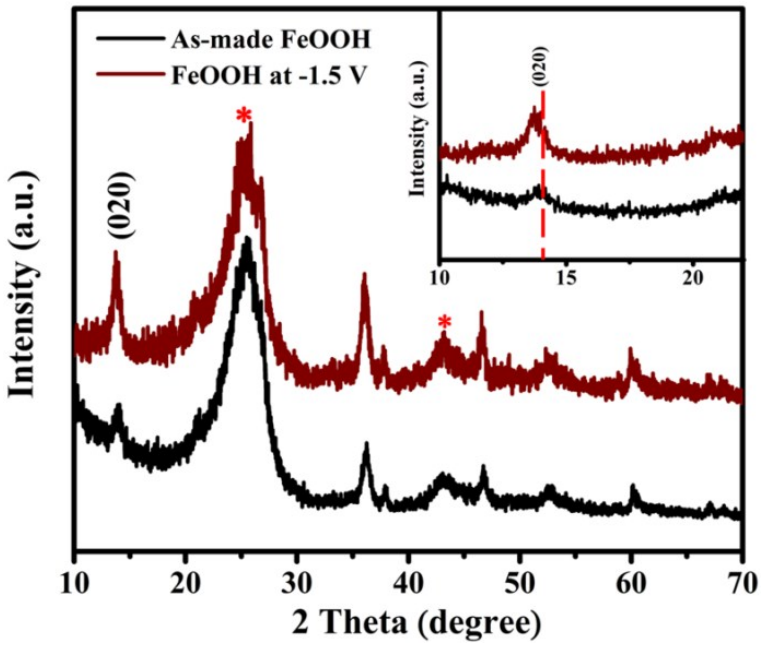

Figure S8. XRD patterns of as-made FeOOH NSs/CC electrode and after discharge proceeding to -1.5 V.

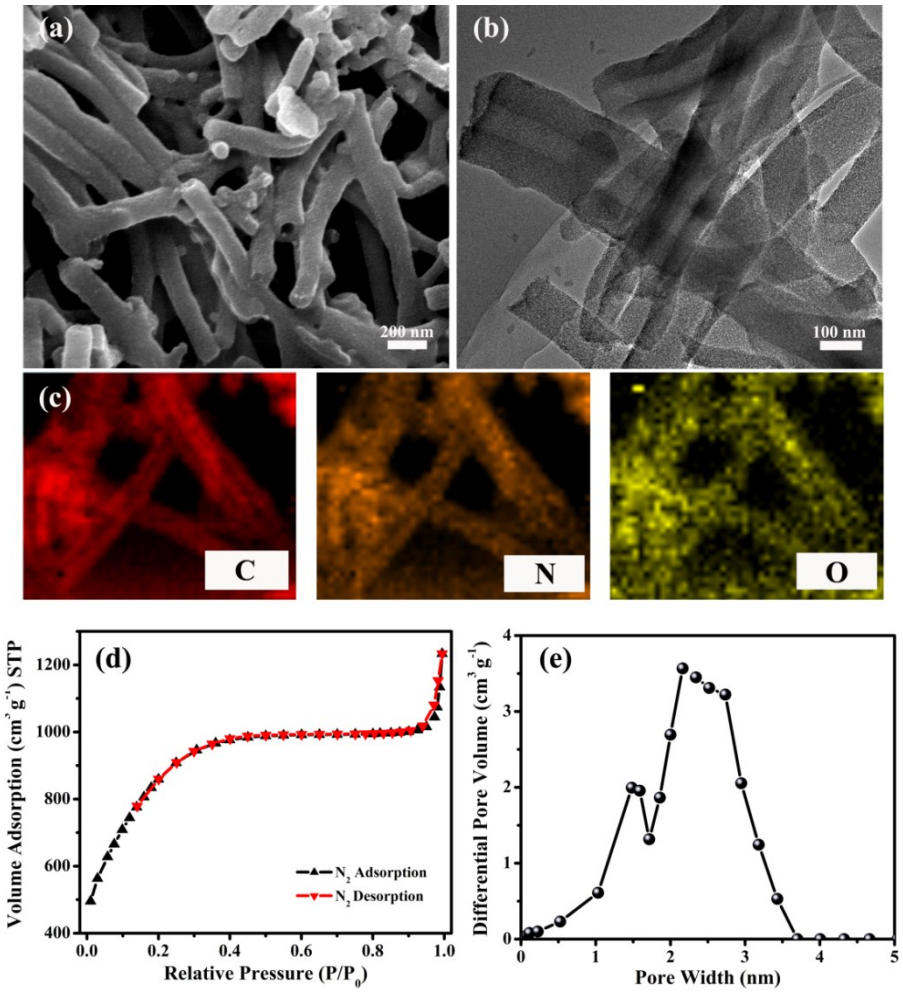

Figure S9. (a and b) SEM and TEM images of the APDC material. (c) The element mappings of APDC corresponding to C, O and N. (d and e) The N_2 sorption isotherms and the corresponding pore size distribution of APDC.

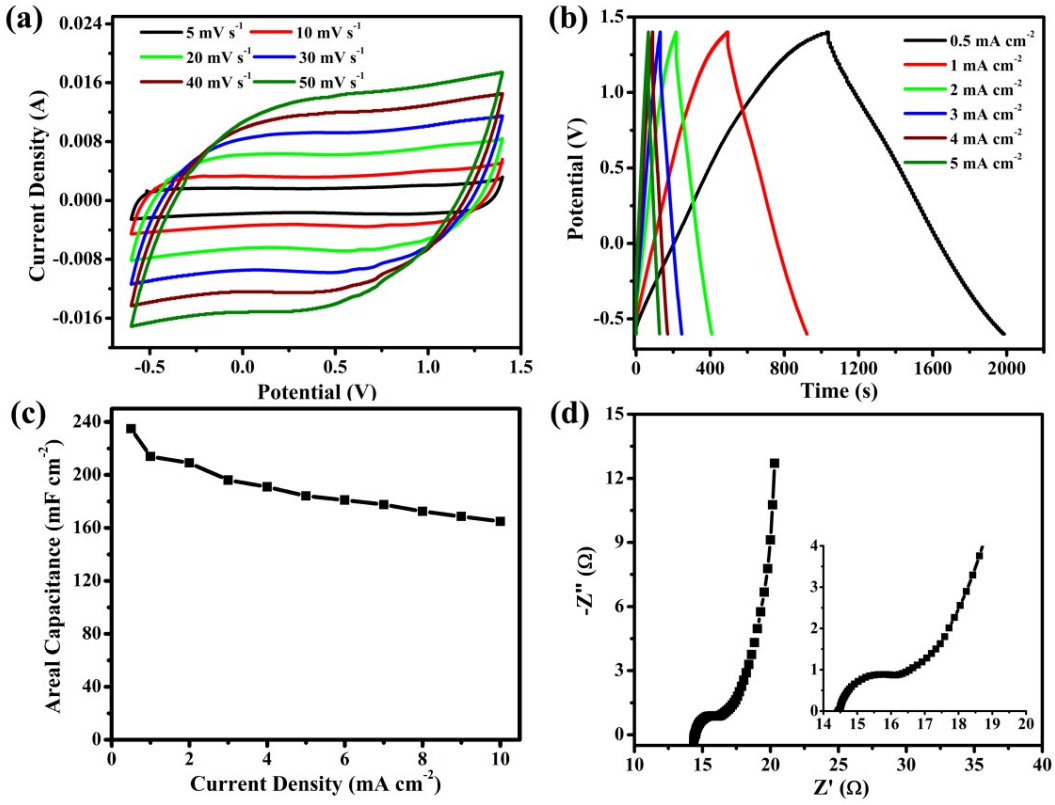

Figure S10. (a) CV curves of the APDC electrode at different scan rates. (b) GCD curves of the APDC electrode at different current densities. (c) The areal capacitance as a function of discharge current density. The loading mass is 1.5 mg cm^{-2}. (d) The Nyquist plot of the APDC electrode. The electrolyte is EMIM-NTF_2 IL.

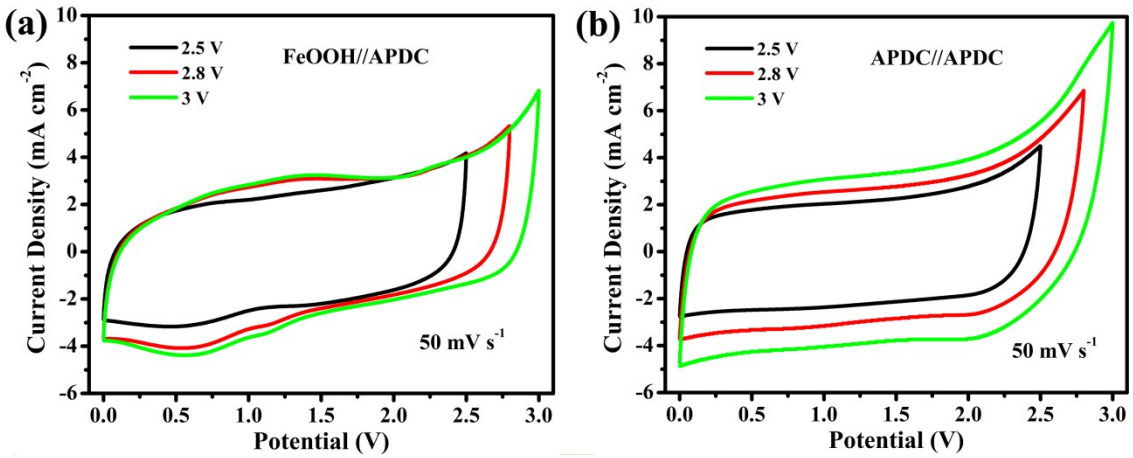

Figure S11 (a) CV curves of FeOOH//APDC asymmetric f-SSC with different operation voltages at the scan rate of 50 mV s^{-1} in EMIM-NTF_2-4 wt% FS ionogel. (b) CV curves of APDC//APDC symmetric f-SSC with different operation voltages at the scan rate of 50 mV s^{-1} in EMIM-NTF_2-4 wt% FS ionogel.

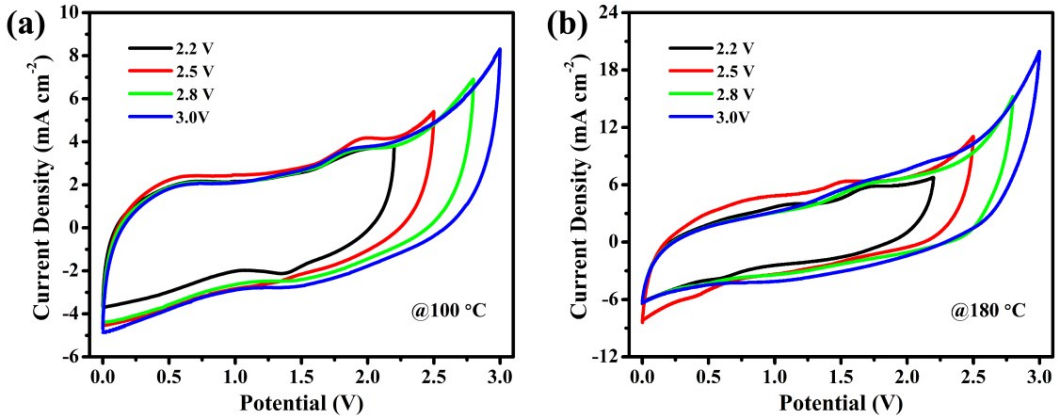

Figure S12. (a and b) CV curves of the FeOOH//APDC f-SSC using EMIM-NTF_2-4 wt% FS ionogel as electrolyte with different operation voltages at the scan rate of 50 mV s^{-1} and at the temperatures of 100 ºC and 180 ºC, respectively.

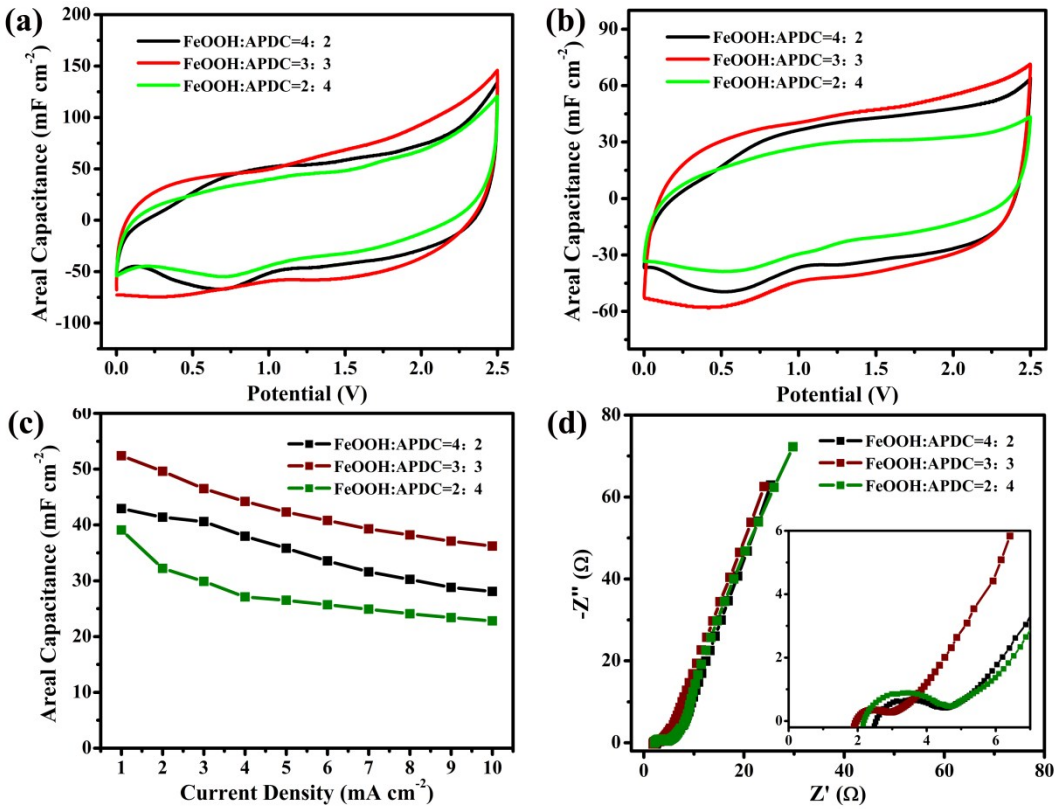

Figure S13. (a and b) CV curves of asymmetric f-SSCs fabricated with different FeOOH/APDC mass ratios at the scan rate of 10 and 100 mV s^{-1}, respectively. (c) Comparison of the areal capacitances of asymmetric f-SSCs fabricated with different FeOOH/APDC mass ratios at the different current densities. (d) The Nyquist plots of asymmetric f-SSCs fabricated with different FeOOH/APDC mass ratios. All the f-SSCs used EMIM-NTF_2-4% FS as ionogel electrolyte.

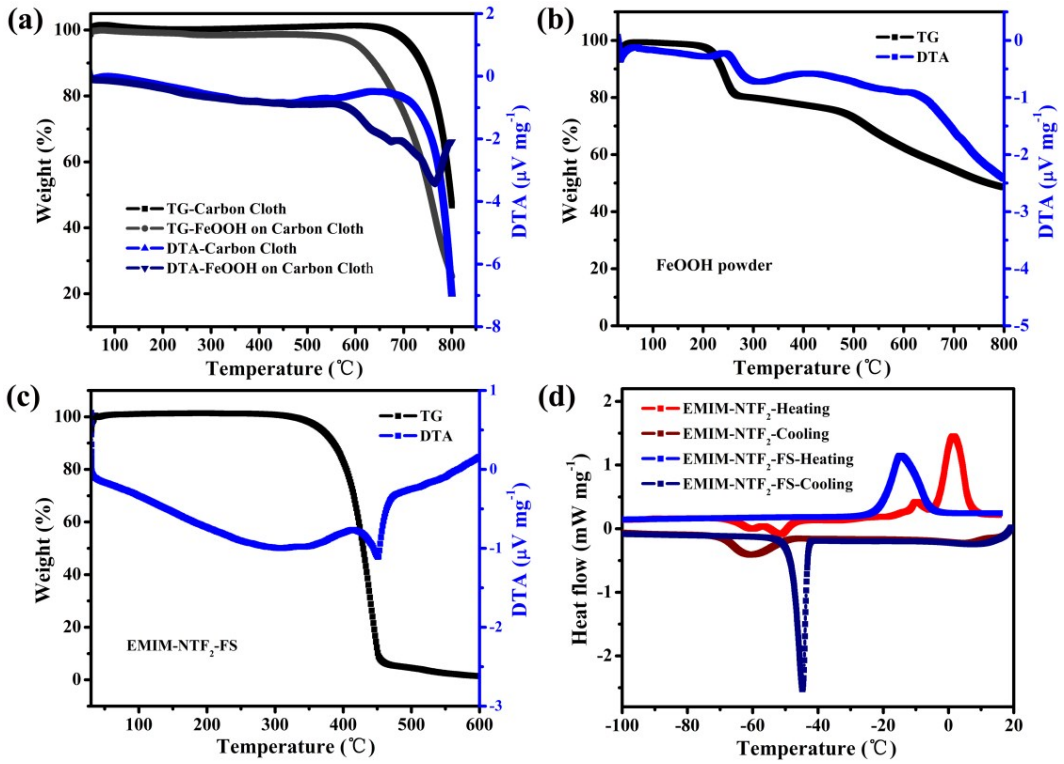

Figure S14. (a and b) TGA and DTA curves for carbon cloth substrate, the FeOOH NSs/CC electrode and the FeOOH powders at the heating rate of 10 °C min^{-1} in air. (c) TGA and DTA curves for the EMIM-NTF_2-4% FS gel electrolyte in air. (d) DSC traces of EMIM-NTF_2 IL and EMIM-NTF_2-4% FS during heating and cooling under N_2 atmosphere, indicating the formation of EMIM-NTF_2-4% FS ionogel.

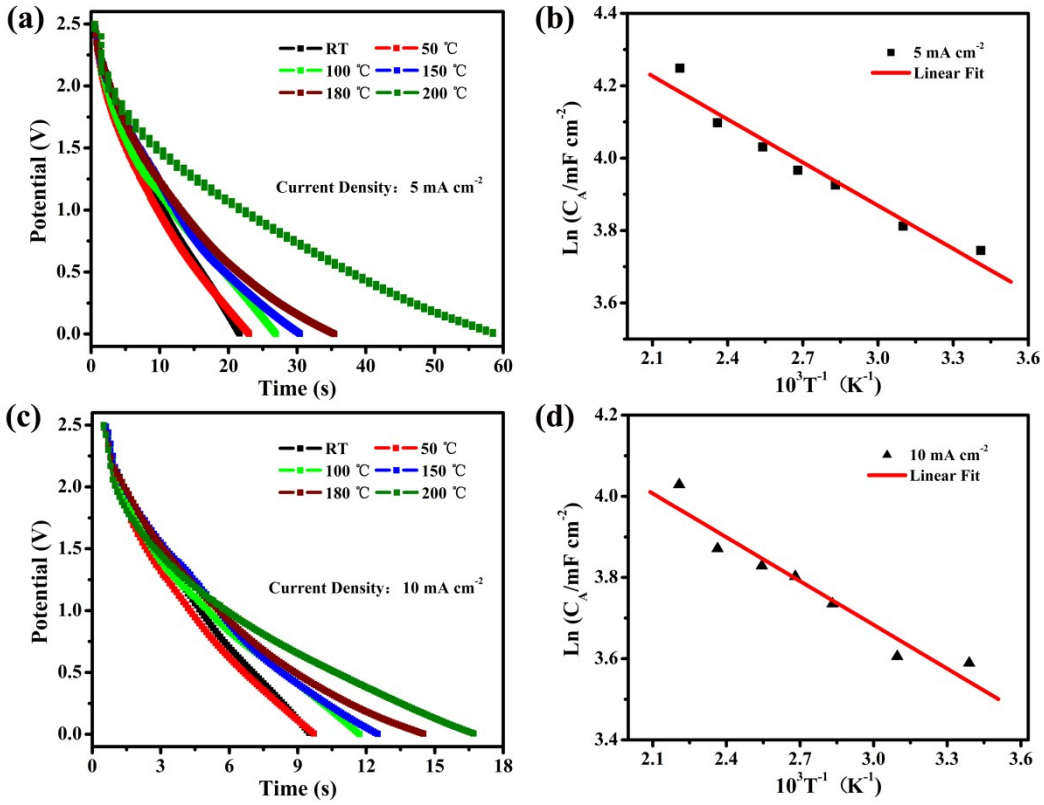

Figure S15. (a and c) Galvanostatic discharge curves of asymmetric f-SSC using EMIM-NTF_2-4% FS as ionogel electrolyte in the range from room temperature to 200 ºC measured at the current densities of 5 mA cm^{-2} and 10 mA cm^{-2}, respectively. (b and d) Arrhenius plots of area capacitance vs. inverse temperature.

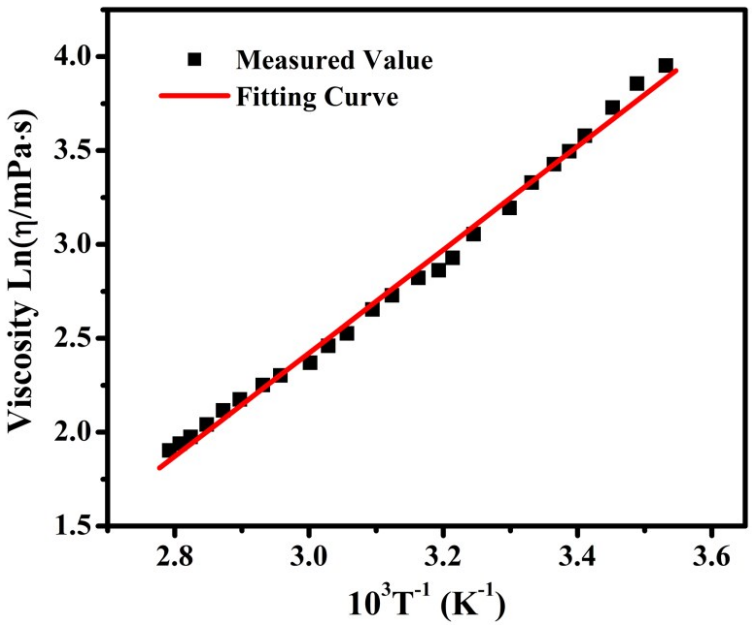

Figure S16. Viscosity of EMIM-NTF_2 IL as a function of temperature.

Figure S16 shows the temperature dependence of the viscosities for EMIM-NTF_2 IL. RT ILs are viscous liquids, and their viscosities exceed 1-3 orders of magnitude higher than those of conventional electrolytes, which is not conducive to electrochemical properties.[1] However, the viscosity (η) of ILs can been significantly reduced through elevating temperature, which is mainly related to the variation of hydrogen bonding. Similar to ionic conductivity, the viscosity of ILs also follows the corresponding VFT equation:[2]

$$\eta = \eta_0 exp\left[\frac{B}{(T - T_0)}\right]$$

where η_0 (mPa·S), B (K), and T_0 (K) are fitting parameters. Through fitting the values of the ionic conductivity of EMIM-NTF_2-FS ionogel and the viscosity of EMIM-NTF_2 IL as a function of temperature, the calculated slopes according to the VFT equations are almost the same, indicating very similar temperature dependence for EMIM-NTF_2-FS ionogel and EMIM-NTF_2 IL.

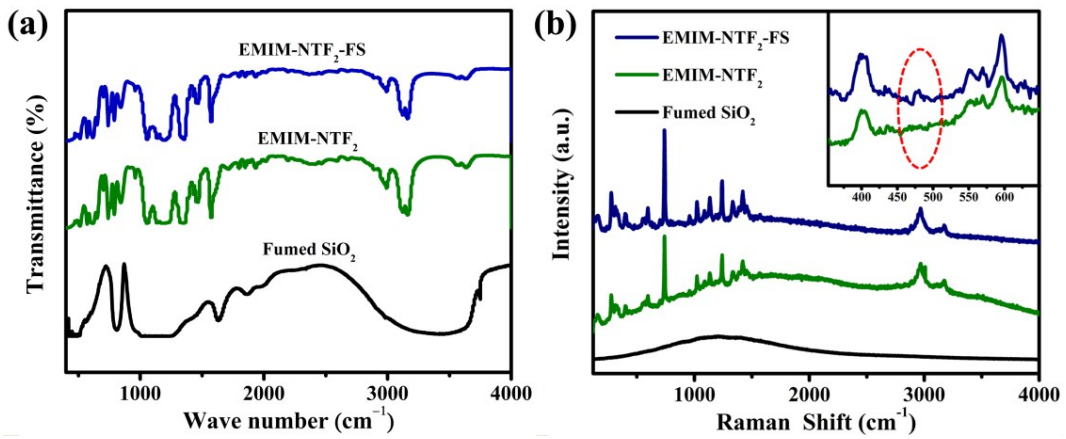

Figure S17. (a) FT-IR and (b) Raman spectra of EMIM-NTF_2-4% FS, EMIM-NTF_2 and Fumed SiO_2 (FS).

As can be seen from the FT-IR spectra above, the characteristic peak of ILs at 1575 cm^{-1} originates from C-C and C-N stretching vibrations of the imidazole ring. Additional bands at 3162, 2989 and 1463 cm^{-1} are attributed to C-H stretching and deformation vibrations of the imidazole moiety and alkyl chain. Moreover, the prominent peak observed at 1056 cm^{-1} can be assigned to the S-O stretching vibration. All of these IL characteristic peaks can also be observed in the IR spectrum of the ionogel EMIM-NTF_2-FS. A broad peak at 1128 cm^{-1} corresponds to the Si-O-Si stretching mode of silica-based ionogels, and a broad feature at 3433 cm^{-1} is ascribed to the Si-OH groups.[3, 4] Based on previous literature,[5] we assign the observed bands at 597, 741, 1332, 1422, 1458, 1574, 2968 and 3175 cm^{-1} to intramolecular vibrations of the nonplanar $[EMIM]^+$.

All characteristic Raman peaks of EMIM-NTF_2 are the same as that in the Raman spectrum of ionogel EMIM-NTF_2-FS except for 475 cm^{-1}. The band at 475 cm^{-1} derives from the planar conformer of $[EMIM]^+$ cation, which has a higher energy (2-4 kJ mol^{-1}) compared with the nonplanar conformer.[6]

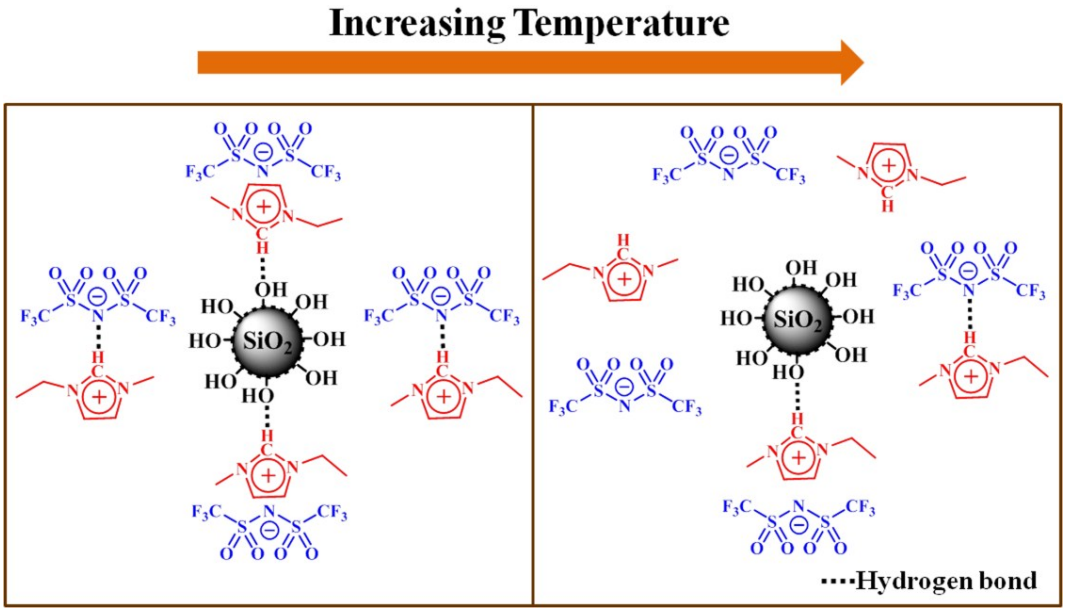

Figure S18. Schematic diagram of interaction mechanism of EMIM-NTF_2-FS ionogel electrolyte with an elevated temperature.

Based on the FT-IR and Raman spectra as shown in Figure S17 and reported literature, [7, 8] Taking the example of hydrogen bonds, we showed the possible schematic diagram and interaction mechanism of EMIM-NTF_2-FS ionogel electrolyte as can be seen from Figure S18. Hydrogen bonds between the C(2)-H of $[EMIM]^+$ and Si-OH groups have formed, as well as the H bonds between cations and anions of ILs. The activation effect resulting from the rise of temperature could partially destroy or weaken H bonds, which would facilitate migration of the cations and anions. Thus, the electrochemical performance would be improved.

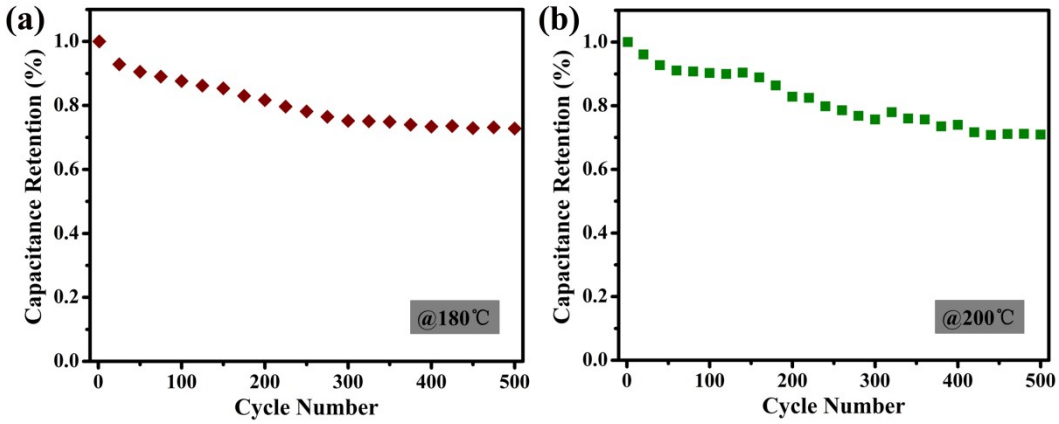

Figure S19. Cycling stability of the FeOOH//APDC f-SSCs at (a) 180 ºC and (b) 200ºC. The capacitance values were calculated based on the CV curves.

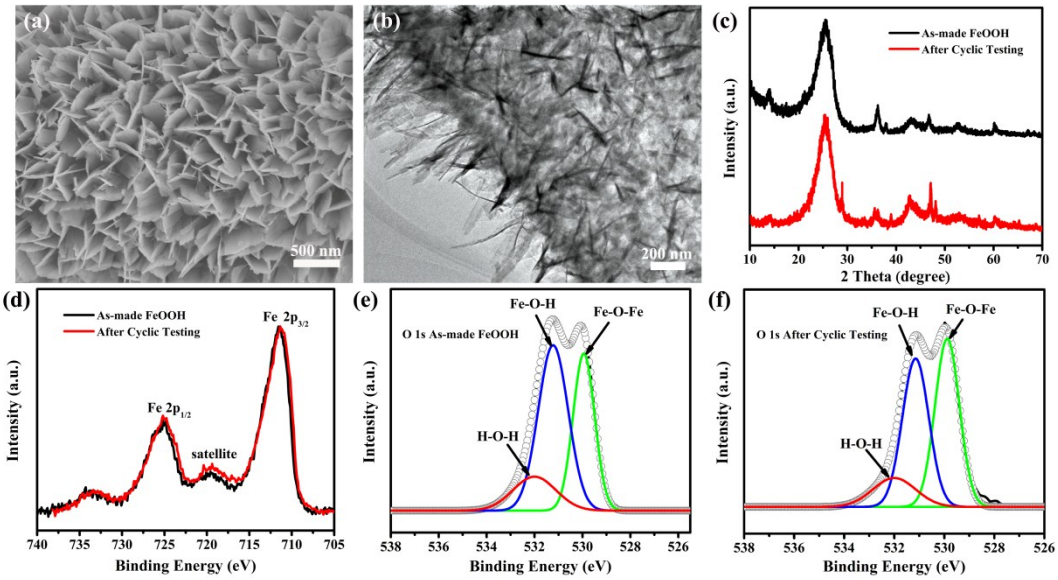

Figure S20. Structure characteristics of the FeOOH NSs/CC electrode in the assembled FeOOH//APDC f-SSC after cyclic testing at 200 ºC for 500 cycles. (a and b) SEM and TEM images before and after cyclic testing. (c) XRD patterns before and after cyclic testing. (d) XPS Fe2p spectra before and after cyclic testing. (e and f) XPS O 1s spectra before and after cyclic testing.

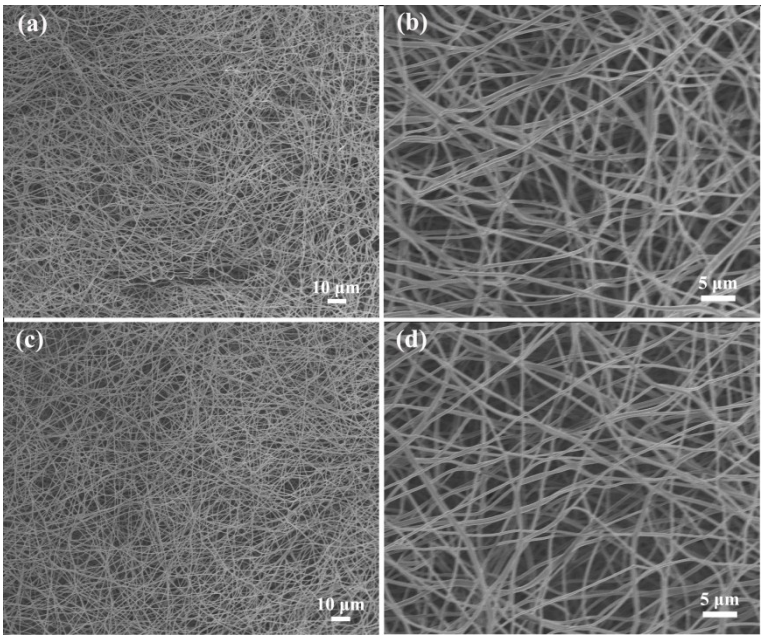

Figure S21. (a, b) SEM images of original polyimide separator under different magnification. (c, d) SEM images of polyimide separator after annealing for 2 h in air at 200 °C.

Separators possessing thermal stability are highly desired to meet the requirement of application in high-temperature supercapacitors. Thermosetting polyimides were known for thermal stability, good chemical resistance and excellent mechanical properties, which were sufficient for a torture of continuous use at temperatures of 230 °C and for short excursions as high as 480 °C.[9] In order to identify whether the porous structures of polyimide separator changed, polyimide films have been characterized by SEM (Figure S21) before and after annealing for 2 h in air at 200 °C. There was no noticeable change in the porous structures of polyimide separator according to Figure S21c and S21d after annealing for 2 h in air at 200 °C. Especially they retained an intact porous structure of polyimide separator, and these porous fiber structures would ensure a better diffusion and transmission of electrolyte ions.

In our research system, we adopted polyimide films as separator to effectively prevent electrical short circuits during bending and applying a force before testing which can improve contact between the electrolyte and electrodes and reduce the contact resistance. In addition, the viscosity of electrolyte can been significantly reduced with elevating temperature according to the viscosity of EMIM-NTF_2 IL as a function of temperature as shown in Figure

S16, and the ionogel electrolyte had a similar variation trend along with temperature. The polyimide films employed as separator could avoid short circuits owing to lower viscosities of the ionogel electrolyte with the rise of temperature when we evaluated the electrochemical performances of f-SSC at high temperatures.

References:

1 S. Zhang, N. Sun, X. He, X. Lu and X. Zhang. *J. Phys. Chem. Ref. Data*, 2006, **35**, 1475-1517.

2 H. Tokuda, K. Hayamizu, K. Ishii, M. A. B. H. Susan and M. Watanabe. *J. Phys. Chem. B*, 2005, **109**, 6103-6110.

3 Q. Zhang, J. Luo and Y. Wei. *Green Chem.*, 2010, **12**, 2246-2254.

4 F. Shi and Y. Deng. *Spectrochimica acta. Part A, Molecular and biomolecular spectroscopy*, 2005, **62**, 239-244.

5 E. R. Talaty, S. Raja, V. J. Storhaug, A. Dölle and W. R. Carper. *J. Phys. Chem. B*, 2004, **108**, 13177-13184.

6 Y. Umebayashi, T. Fujimori, T. Sukizaki, M. Asada, K. Fujii, R. Kanzaki and S.-i. Ishiguro. *J. Phys. Chem. A*, 2005, **109**, 8976-8982.

7 K. Dong, S. Zhang, D. Wang and X. Yao. *J. Phys. Chem. A*, 2006, **110**, 9775-9782.

8 B. Shen, J. Lang, R. Guo, X. Zhang and X. Yan. *ACS Appl. Mater. Interfaces*, 2015, **7,** 25378-25389.

9 W. Jiang, Z. Liu, Q. Kong, J. Yao, C. Zhang, P. Han, G. Cui, *Solid State Ionics*, 2013, **232**, 44-48.